Materials Performance and Characterization

M. R. Rahul[1] and G. Phanikumar[2]

DOI: 10.1520/MPC20140065

Correlation of Microstructure With HAZ Welding Cycles Simulated in Ti-15-3 Alloy Using Gleeble 3800 and SYSWELD

Copyright by ASTM Int'l (all rights reserved); Fri Aug 14 09:36:56 EDT 2015
Downloaded/printed by
Indian Inst of Tech Chennai (Indian Inst of Tech Chennai) pursuant to License Agreement. No further reproductions authorized.

Materials Performance and Characterization

doi:10.1520/MPC20140065 available online at www.astm.org

M. R. Rahul[1] and G. Phanikumar[2]

Correlation of Microstructure With HAZ Welding Cycles Simulated in Ti-15-3 Alloy Using Gleeble 3800 and SYSWELD

Reference

Rahul, M. R. and Phanikumar, G., "Correlation of Microstructure With HAZ Welding Cycles Simulated in Ti-15-3 Alloy Using Gleeble 3800 and SYSWELD," *Materials Performance and Characterization* doi:10.1520/MPC20140065. ISSN 2165-3992

ABSTRACT

Metastable β-titanium alloys are finding increasingly wider applications in structural components in aerospace, energy, and chemical industries because of their formability and heat-treatment possibilites. Components from these alloys are usually welded by processes, such as gas tungsten arc welding (GTAW), electron beam welding (EBW), and laser beam welding (LBW). Post-weld heat treatment improves the strength of the weld because of the precipitation of α phase and $TiCr_2$ particles. In β-titanium alloys, the location, distribution and morphology of α precipitates in β matrix plays an important role in the performance of the welded components. In this work, we simulate different welding processes using Sysweld software and obtain realistic thermal cycles after calibrating the fusion zone dimensions with known experimental data. These cycles are then used to program the heat-affected zone (HAZ) cycles in Gleeble 3800 to study their effect on the microstructure of the β-titanium alloy. Both continuous and pulsed welding conditions are used for the welding process. Microstructure characterization was performed using scanning electron microscopy (SEM), electron back-scattered diffraction (EBSD), and transmission electron microscopy (TEM). Precipitates of α phase below 0.2 μm are seen to be uniform across the β grain but the number density is not uniform across different grains of β. We discuss the characterization results in light of existing models in the literature. The α

Manuscript received December 31, 2014; accepted for publication July 9, 2015; published online August 3, 2015.

[1] Research Scholar, Dept. of Metallurgical and Materials Engineering, Indian Institute of Technology Madras, Chennai 600036, India.

[2] Associate Professor, Dept. of Metallurgical and Materials Engineering, Indian Institute of Technology Madras, Chennai 600036, India (Corresponding author), e-mail: gphani@iitm.ac.in

Copyright © 2015 by ASTM International, 100 Barr Harbor Drive, P.O. Box C700, West Conshohocken, PA 19428-2959

Copyright by ASTM Int'l (all rights reserved); Fri Aug 14 09:36:56 EDT 2015
Downloaded/printed by
Indian Inst of Tech Chennai (Indian Inst of Tech Chennai) pursuant to License Agreement. No further reproductions authorized.

precipitation and hardness variation are correlated with welding cycles. A combination of computational and physical simulation tools is proposed to reduce the cycle to find optimal choice in the fabrication process design space.

Keywords

FEM simulation, physical simulation, precipitation

Introduction

Weldability is an important aspect in the design of alloys. Fabrication of complex geometrical parts from individual parts involves welding as a process step that could significantly alter the part characteristics [1]. Thermal cycles resulting from the welding processes could alter the final microstructure and also lead to residual stresses and distortions. Repair and refurbishment of investment/directionally cast parts also involves variants of welding processes, such as weld overlay. Thus, for both wrought and cast components of a newly designed alloy, weldability is an aspect that needs to be evaluated as part of the design process. In this study, we take up the case of welding of metastable β-titanium alloys [2] and illustrate the role played by thermal profiles in the final microstructure of the weld. Based on this study, a modification of the workflow of design process is suggested toward accelerated design of alloys.

Titanium alloys are widely used in aerospace, energy, chemical and biomedical industries. Because of their excellent mechanical properties, β Ti alloys have become a choice of alloys that combine good formability with the possibility of improvement of strength through heat treatment. Ti-15-3 alloy has excellent cold deformability in a solution-treated condition and its properties could be improved by aging [3]. Weld thermal cycles are known to lead to significant changes in the microstructure and mechanical properties of these alloys [4].

The transformation temperature in pure Ti from body-centered-cubic (β) to hexagonal-closed-packed (α) phase transformation during cooling below 882°C can be controlled by the addition of β and α stabilizing agents [5]. Elements such as Mo, V, Nb, and Cr act as β stabilizing agents, and Al will act as an α stabilizing agent and change the transformation temperature. To stabilize β phase on quenching, a Mo equivalency of more than 10 at. % is required [6]. The alloy used in the present study is Ti-15-3, having a Mo equivalency of 11.85 at. % and has a β phase at room temperature.

Ti and its alloys are commonly welded by gas tungsten arc welding (GTAW), gas metal arc welding (GMAW), laser beam welding (LBW), electron beam welding (EBW), and plasma arc welding (PAW) [7,8]. It is reported that metastable β Ti alloys are readily weldable; the fusion zone consists of columnar grains and the heat-affected zone (HAZ) consists of retained β grains [6]. GTAW is an established welding technique for β Ti alloys [9]. The as-welded condition for most of β Ti alloys leads to good ductility and relatively less strength, usually lower than that of base metal [10]. To improve the strength, heat treatment can be carried out but that would also lower the ductility [6]. Pulsed GTAW and effects of pulsing frequency on

Copyright by ASTM Int'l (all rights reserved); Fri Aug 14 09:36:56 EDT 2015
Downloaded/printed by
Indian Inst of Tech Chennai (Indian Inst of Tech Chennai) pursuant to License Agreement. No further reproductions authorized.

welding of Ti-15-3 alloy were studied by Balachandar et al. [4], wherein they reported the precipitation of α phase in the as-welded condition for both continuous current and pulsed current conditions.

Numerical techniques can be used to simulate the welding process and to find the approximate residual stresses in the weldment. A finite element package, Sysweld, can be used to simulate the bead on plate weld [11] as well as for complex geometries. A double ellipsoidal model is often used to define the heat source. The parameter fitting can be done considering the actual weld dimensions and thermal cycles.

Physical simulation of material processing involves the exact reproduction of the thermal and mechanical conditions in the laboratory that the material is subjected to in the actual fabrication process or end use. HAZ simulation in Gleeble 3800 is widely used in steels, Ni-based alloys [12], and in Ti alloys to correlate the welding parameters with microstructure. The narrow HAZ microstructure is replicated in a wide area in the simulated sample.

Various thermomechanical cycles are reported for processing β-titanium alloy for better strength. Precipitation time temperature diagram are also established [3]. Formation of ω phase is reported to act as a possible precursor for α precipitation. The rate of heating to the aging temperature also has a profound effect on the precipitation of α phase. Precipitate-free zones and grain boundary α are also reported [13]. The mechanism of α nucleation and growth are established in β Ti alloys shows that α precipitates in the interior of grain boundaries latter impingement will occur to form a continuous layer. Salib et al. [14] also reported a mechanism for precipitation in β Ti-17 alloy.

In this study, we report our work using both the finite element software package Sysweld and physical simulation system Gleeble 3800 to simulate HAZ for realistic welding cycles. Verifying the formation of precipitates was done using detailed characterization techniques. The pulsed current welding cycle is simulated, and the distance at which the pulsing effect is negligible was determined for different welding conditions. The α precipitation was correlated with the current open literature.

Numerical Simulation

Sysweld is an industry standard of the FEM package, which is known to provide realistic welding simulation of thermal profiles, residual stresses, and distortion calculations for complex geometries. Using eight node cube elements, a 3D model of Ti plate was created in the visual weld pre-processor (**Fig. 1(*a*)**). To give a pulsing effect, the model is scaled down from the actual plate dimension. Adaptive meshing is used to create the fine element mesh. To reduce the computational time and capture the thermal profile accurately in the fusion zone and heat-affected zone, a finer meshing was used. In the regions away from the weld zone, a coarser mesh was used. Quadrilateral elements are used for the transition region from fine to coarse mesh (**Fig. 1(*b*)**). Input parameters for 3D models, such as specific heat and thermal conductivity, both varying with temperature and density, are given based on the literature [8]. The 3D model of the Ti plate was created for modeling, and the resulting thermal profile generated was used for physical simulation of HAZ.

Copyright by ASTM Int'l (all rights reserved); Fri Aug 14 09:36:56 EDT 2015
Downloaded/printed by
Indian Inst of Tech Chennai (Indian Inst of Tech Chennai) pursuant to License Agreement. No further reproductions authorized.

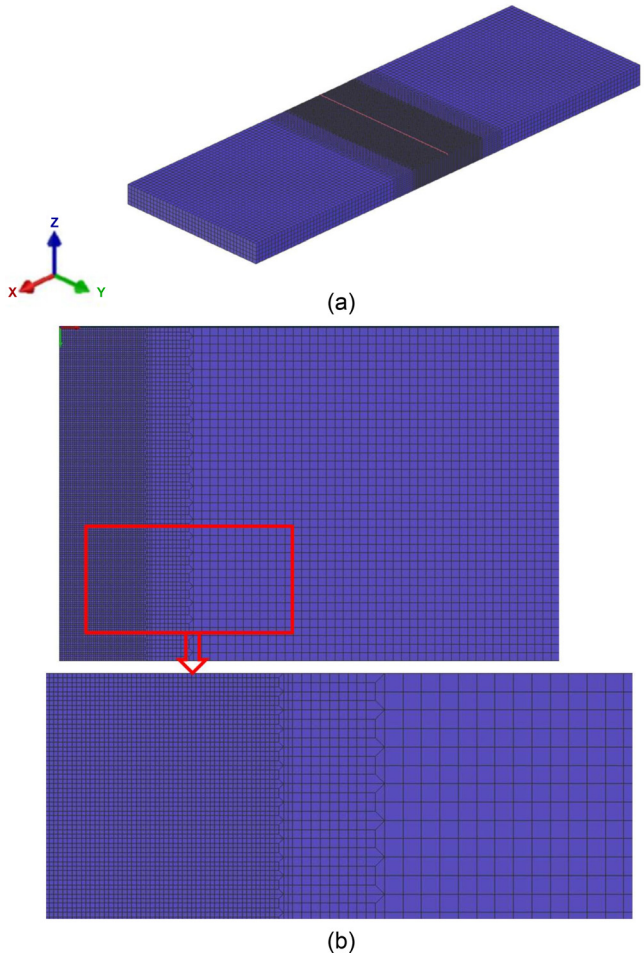

FIG. 1
(*a*) 3D mesh of Ti plate (120 mm × 40 mm × 5 mm) and (*b*) mesh in the transition region along with a magnified version of the inset.

HEAT SOURCE FITTING (HSF) TOOL

Different heat source models available for the welding simulation are listed in **Table 1** [15]. More accurate results will require using more complex heat source models. A heat source–fitting tool was used to determine the heat source parameters. The double ellipsoidal model defined by Goldak and co-workers [16] was used for simulating both continuous current and pulsed current tungsten inert gas (TIG) welding (**Fig. 2**). The actual weld macrograph and thermal cycle collected by using thermocouples at different locations are used for calibrating the heat source parameters. The pulsing effect was given to the heat source by varying the heat intensity with time along the weld line. The cooling of the plate is done by using convection with air and the convective heat-transfer coefficient used are shown in **Table 2**.

As shown in the literature, the front half of the Goldak double ellipsoidal model is the quadrant of one ellipsoidal heat source and the rear half is another quadrant of the heat source. Equations 1–3 are used by Sysweld to define the power density on the inside, the front, and the rear end, respectively [16].

Copyright by ASTM Int'l (all rights reserved); Fri Aug 14 09:36:56 EDT 2015
Downloaded/printed by
Indian Inst of Tech Chennai (Indian Inst of Tech Chennai) pursuant to License Agreement. No further reproductions authorized.

TABLE 1

Classification of current welding heat source model [15].

Mode	One Dimension	Two Dimension	Three Dimension
Uniform distribution mode	Point heat source	Plane heat source	Columnar heat source
	Line heat source	Circular mode	
		Tripped heat source	
		Square heat source	
		Circular mode	Circular disk heat source
		Oval-shaped heat source	Columnar heat source
		Double oval-shaped heat source	Cuboid heat source
		Tripped heat source	Rotary body heat source
Gaussian mode			Conic heat source
			Hemispherical heat source
			Semi ellipsoidal heat source
			Ellipsoidal heat source
			Double ellipsoidal heat source
Exponential decay mode			Exponential decay heat source
Dynamic heat source mode			Composed of parabolic and Gaussian mode

$$q_f(x,\xi,z,t) = \frac{6\sqrt[2]{3}Q_f}{a_f bc\pi\sqrt{\pi}} \cdot e^{\frac{-3x^2}{a_f^2}} \cdot e^{\frac{-3\xi^2}{b^2}} \cdot e^{\frac{-3z^2}{c^2}} \quad (1)$$

$$q_r(x,\xi,z,t) = \frac{6\sqrt[2]{3}Q_r}{a_r bc\pi\sqrt{\pi}} \cdot e^{\frac{-3x^2}{a_r^2}} \cdot e^{\frac{-3\xi^2}{b^2}} \cdot e^{\frac{-3z^2}{c^2}} \quad (2)$$

$$\xi = y - v(\tau - t) \quad (3)$$

where:

a_f, a_r, b, c = the radial dimensions in front length, rear length, width of molten zone, and depth of molten zone, respectively, and

Q_f and Q_r = the front and rear source intensity parameters, respectively. For defining the position of the heat source at $t = 0$, we used t (the lag factor).

To achieve the best fit, the heat source parameters are varied in an iterative manner.

FIG. 2

Goldak double ellipsoidal heat source model [14].

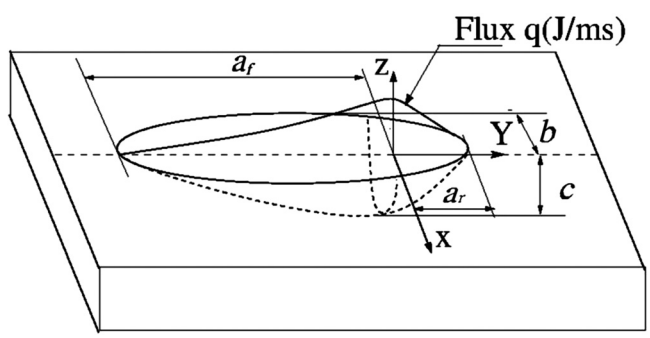

Copyright by ASTM Int'l (all rights reserved); Fri Aug 14 09:36:56 EDT 2015
Downloaded/printed by
Indian Inst of Tech Chennai (Indian Inst of Tech Chennai) pursuant to License Agreement. No further reproductions authorized.

TABLE 2

Convective heat-transfer coefficients used for simulation.

Temperature (°C)	Convective Heat-Transfer Coefficient ($W/m^2/K$)
20	60
100	60
200	65
300	205
400	290
500	370
600	450
700	490
800	505
900	530
1000	640
1200	900
1400	950
1600	975
2000	1000
2500	1100
3000	1150
4000	1175

The actual welding speed, 2.5 mm/s, which will give the optimum weld quality, is selected as the torch velocity and the welding variables taken from actual welding condition [voltage 13.6 V and current (for continuous current 150 A and pulsed current TIG peak current 190 A and base current 110 A)]. For giving the pulsing effect, the intensity is varied according to the actual square wave that represents the variation of current. The pulsing effect is simulated for different frequencies (4 Hz and 6 Hz). The thermal cycles at different locations are plotted to determine the distance beyond which the effect of pulsing in thermal cycle can be neglected. The thermal cycle at different locations plotted for use as input to the physical simulation using Gleeble are shown in **Fig. 3(*a*)–3(*c*)**.

Experiments

Samples were made from rectangular plates of dimension 120 mm by 25 mm by 2 mm with holes drilled at the ends according to the standard dimensions prescribed in the Gleeble manual. The sample composition was verified using inductively coupled plasma–optical emission spectrometry (ICP-OES) and energy dispersive spectrometer (EDS) attachment to SEM. The composition measured in wt. % is 77.4 % Ti + 13.7 % V + 3.5 % Al + 1.9 % Cr + 3.5 % Sn.

In actual welding processes, the HAZ is narrow and difficult to study in detail. By using Gleeble, one can simulate the HAZ to a large-scale sample. The high heating rate of welding can be easily achieved as the sample is heated by resistance. The standard plate sample was taken and held using stainless steel or Cu grips based on the required cooling rate as shown in **Fig. 4**. The temperature control is done by

Copyright by ASTM Int'l (all rights reserved); Fri Aug 14 09:36:56 EDT 2015
Downloaded/printed by
Indian Inst of Tech Chennai (Indian Inst of Tech Chennai) pursuant to License Agreement. No further reproductions authorized.

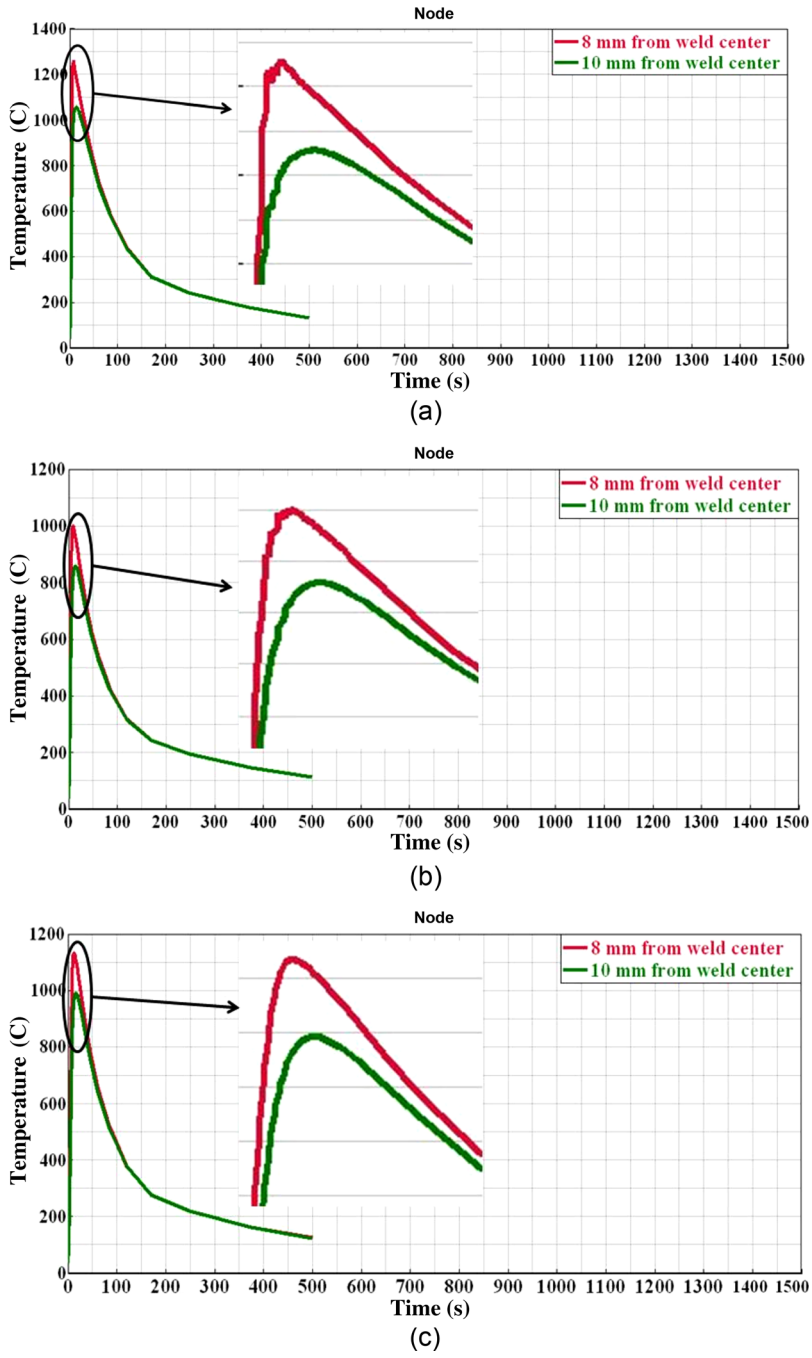

FIG. 3
(*a*) Thermal cycle for 4-Hz pulsed TIG at 8 and 10 mm from center, (*b*) thermal cycle for 6-Hz pulsed TIG at 8 and 10 mm from center, and (*c*) thermal cycle for continuous current TIG at 8 and 10 mm from center.

using a B type thermocouple welded on the center of the sample using a thermocouple spot-welding machine. To find the temperature variation from the center to the ends of the sample, three thermocouples are welded at a distance of 10 mm and 3 mm from the center, respectively. The temperature variation between ±3 mm is less than 10°C.

Copyright by ASTM Int'l (all rights reserved); Fri Aug 14 09:36:56 EDT 2015
Downloaded/printed by
Indian Inst of Tech Chennai (Indian Inst of Tech Chennai) pursuant to License Agreement. No further reproductions authorized.

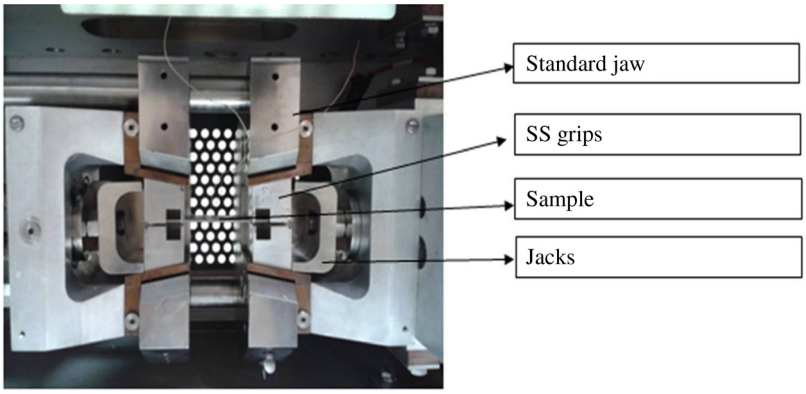

FIG. 4
Mounting of the sample in standard jaws on the thermomechanical simulator.

To simulate realistic cycles, the table program in the Quick-Sim software in-built in the Gleeble 3800 was used. The input data for these thermal cycles were obtained from the Sysweld software. The sample is mounted on the standard jaw with an argon atmosphere in the pocket jaw module. First sample is solutionized at 800°C for 15 min. To avoid the thermocouple detachment at high temperatures, we used bonding cement at the thermocouple junction. The programmed HAZ cycle was simulated at the zero force condition.

The simulated samples are characterized using optical and electron microscopy. Backscattered electron (BSE) imaging and secondary electron (SE) imaging are carried out in FEI quanta 400 and Inspect F interfaced with a TSL–OIM EBSD analysis system and a high-speed Hikari camera. The sample is mechanically and electrolytically polished for EBSD analysis. The EBSD maps are obtained with a step size of 1 or 0.1 μm and indexing both α and β phases. In the orientation maps, different colors represent the different crystallographic orientations of respective phases in the sample. The samples were mechanically polished and etched with Kroll's reagent for 5 to 10 s for SEM-BSE imaging. Transmission electron microscopy (TEM) was conducted for selected samples to verify the precipitate phase.

Microhardness testing was carried in the simulated sample with a load of 500 g and a dwell time of 15 s. The TIG-welded Ti-15-3 plates are taken and the transverse cross section is polished and macro-etched. The macrograph is used for calibrating the HSF and comparing the simulated profiles.

Results

Figure 5(*a*) and **5(*b*)** show the isometric view of maximum temperature contour and torch moving in the simulated sample. To find the weld pool geometry, the liquidus temperature of the alloy is taken as 1659°C. **Figure 6** shows the comparison of weld pool geometry and actual weld geometry (section taken at the center along the weld line and the red line in the macrograph indicating the fusion zone boundary). The peak temperature for the actual thermal cycle and simulated thermal cycle at a distance of 9 mm from the center of weldment is compared and found to be satisfactory. The pulsing effect on the thermal cycle is nullified between 9 to 9.25 mm and 8.5 to 9 mm in the 4 Hz and 6 Hz pulsed condition, respectively.

Copyright by ASTM Int'l (all rights reserved); Fri Aug 14 09:36:56 EDT 2015
Downloaded/printed by
Indian Inst of Tech Chennai (Indian Inst of Tech Chennai) pursuant to License Agreement. No further reproductions authorized.

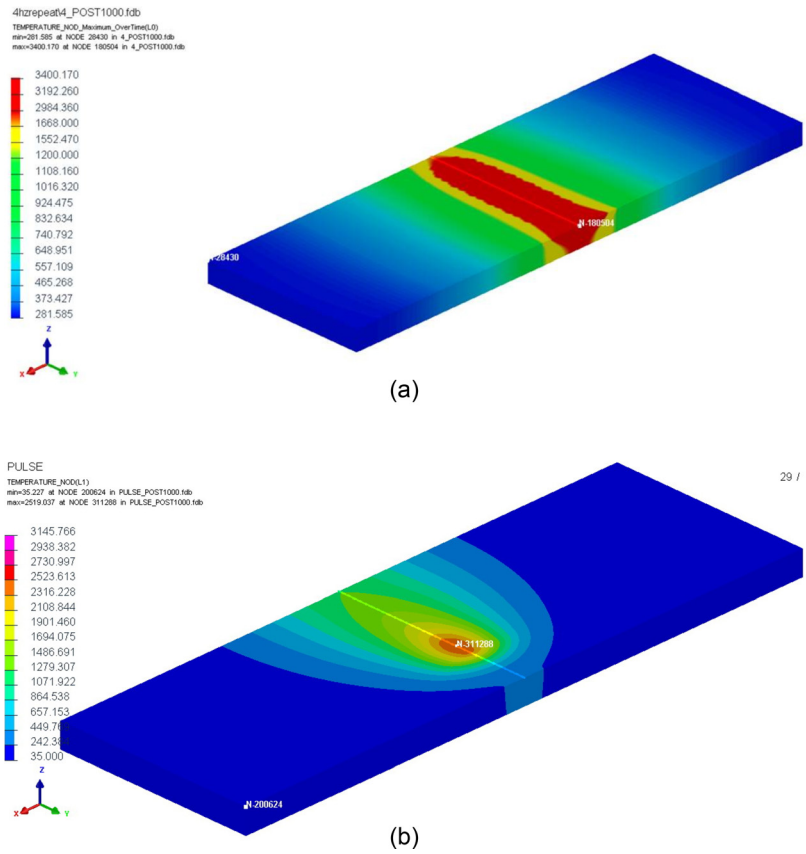

FIG. 5
(*a*) Isometric view max temperature contour of 4-Hz pulsed weld and (*b*) torch moving in continuous current TIG welding.

The thermal profile of the HAZ shown in **Fig. 3** is then used as input for HAZ simulation in the plate sample using Gleeble 3800. **Figure 7** shows the thermal profile of the simulated sample and the programmed thermal cycle. Both are comparable, and the pulsing effect in the thermal cycle is followed by the actual thermal cycle on the simulated sample (reading from thermocouple TC1).

Figure 8 shows the SEM-BSE image for the HAZ-simulated sample at various conditions. BSE images show that most of the grain-boundary precipitates are originating at the triple junction rather than the middle of the grain boundary. The SEM-EDS point analysis shows that there is an enrichment of tin and depletion of vanadium in the grain boundaries where the precipitates are formed (**Fig. 9**). To confirm the precipitates, TEM was used. As can be seen in **Fig. 10**, some of the precipitates are of nanoscale. These are beyond the resolution limit of the SEM-EBSD used in this study. The EBSD analysis shows (**Figs. 11** and **12**) that the proportion of α precipitates seems to vary across different β grains and not uniformly distributed throughout the sample. However, in the grains where the precipitation was observed, it was uniformly distributed within the grain. It is observed that the grain size for the HAZ-simulated sample is large and of the order of 80 to 200 μm. The EBSD orientation image shows the variation of microstructure in pulsed thermal cycles and continuous thermal cycles. It is clear from EBSD orientation image that the grain

Copyright by ASTM Int'l (all rights reserved); Fri Aug 14 09:36:56 EDT 2015
Downloaded/printed by
Indian Inst of Tech Chennai (Indian Inst of Tech Chennai) pursuant to License Agreement. No further reproductions authorized.

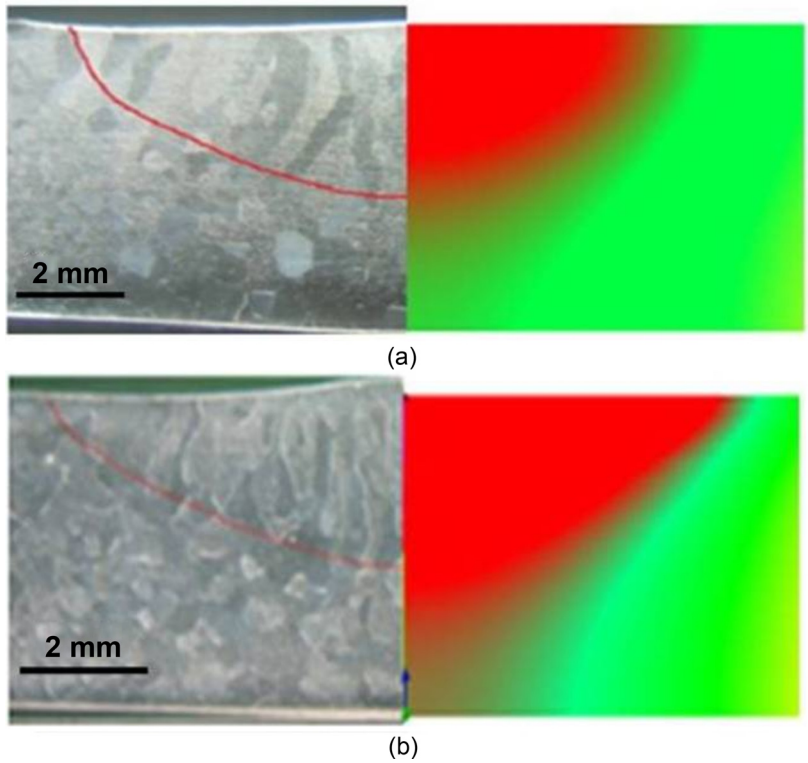

FIG. 6
Comparison of actual weld geometry and simulated weld geometry for (*a*) continuous current and (*b*) pulsed current 4-Hz TIG welding.

boundaries in most of the conditions are decorated by the α precipitates. The precipitates are not uniformly distributed along grains (**Figs. 11** and **12**).

The measured microhardness data is shown in **Table 3**. It can be noted that samples with coarser β grain size have lesser hardness. The increased hardness in 8 mm, and the 4-Hz pulsed thermal cycle is attributed to the formation of precipitates. Samples showing significant α precipitation exhibited higher hardness. The large scatter in the hardness data is attributed to the inhomogeneous distribution of α precipitation across different β grains in the sample. In case of a 4-Hz pulsed current condition, the microhardness values are more at 8 mm compared to 10 mm away from the weld centerline—likely because of a combination of pulsing and a longer stay at higher temperatures similar to the continuous current 8-mm thermal cycle.

Discussion

Because of low thermal diffusivity of β Ti alloys, the diffusion distance for the melting portion in welding need to be calculated. In pulsed welding, it is reported that there exists a combination of diffusion distance, and the distance traversed by the torch in one cycle of the pulse will cause accumulation of heat in HAZ and lead to a high thermal gradient [4]. Such a coupling phenomenon will affect the microstructure and plays a role in the post-weld heat treatment. In Sysweld simulation, we observed that the distance up to which the pulsing effect is pronounced decreases with increase in pulsing frequency.

Copyright by ASTM Int'l (all rights reserved); Fri Aug 14 09:36:56 EDT 2015
Downloaded/printed by
Indian Inst of Tech Chennai (Indian Inst of Tech Chennai) pursuant to License Agreement. No further reproductions authorized.

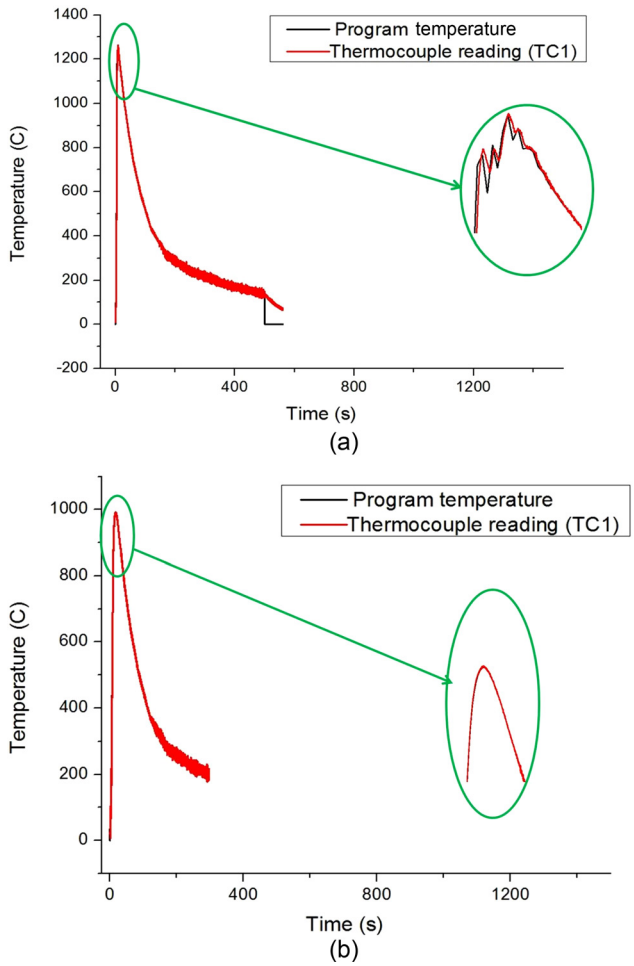

FIG. 7
Graph showing the thermocouple reading from simulated sample (TC1) and program temperature at (*a*) 8 mm from center in 4-Hz pulsed and (*b*) 10 mm from center in continuous current TIG welding.

The literature reports various studies on β Ti alloys that agree that α precipitation occurs at the grain boundaries and then in the interior of the grains. On isothermal aging, the precipitates formed along the grain boundaries will grow to a critical width, and beyond that they will change over to Widmanstätten morphology. From the SEM-BSE imaging, it is clear that the precipitation starts at the triple junction of grain boundaries rather than the center of grain boundaries.

In the **Fig. 13**, a schematic superposition of a weld cooling cycle and a continuous cooling transformation (CCT) diagram of metastable β-titanium alloy is shown. As can be noted, the cooling curve crosses the curves for the initiation of grain boundary α phase before the grain interior α phase for almost any cooling rate that could be chosen. This possibility is corroborated by the experimental characterization results described above. Whereas isothermal heat treatment comprised of various steps and holding times could perhaps rid the grain boundary α phase formation, it is clear here that such a possibility is not offered by the weld-cooling cycles. Choice of the welding process conditions based on the final microstructure and mechanical properties should take this aspect into account.

Copyright by ASTM Int'l (all rights reserved); Fri Aug 14 09:36:56 EDT 2015
Downloaded/printed by
Indian Inst of Tech Chennai (Indian Inst of Tech Chennai) pursuant to License Agreement. No further reproductions authorized.

FIG. 8 SEM-BSE images shows the formation of precipitates: (*a*) continuous current condition (thermal cycle at 8 mm), (*b*) pulsed current condition (4 Hz, thermal cycle at 8 mm), and (*c*) pulsed current condition (4 Hz, thermal cycle at 8 mm with reduced cooling rate).

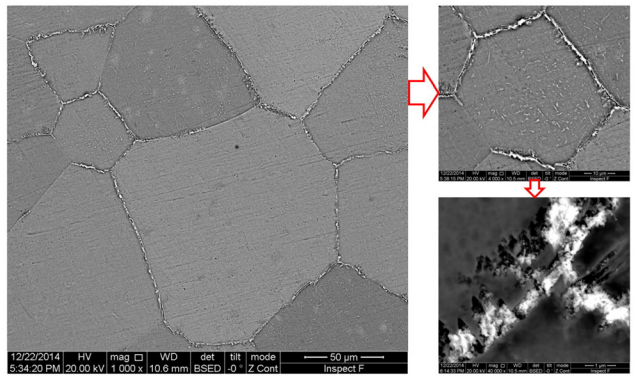

(a)

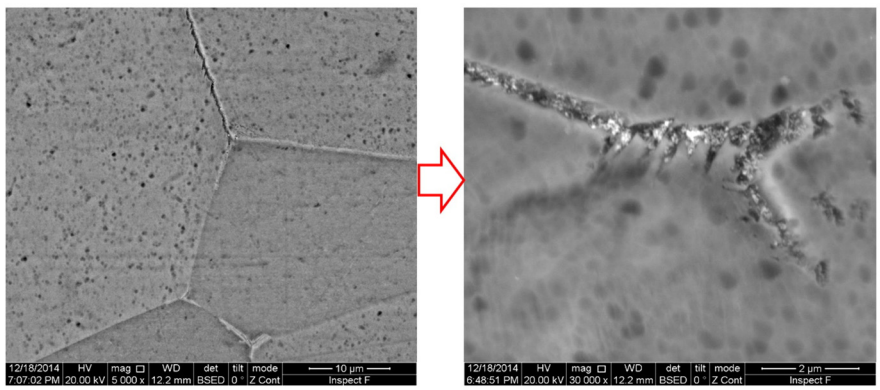

(b)

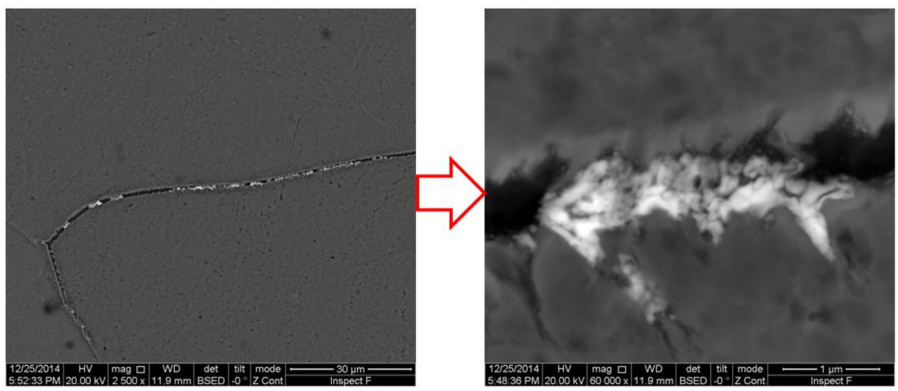

(c)

Copyright by ASTM Int'l (all rights reserved); Fri Aug 14 09:36:56 EDT 2015
Downloaded/printed by
Indian Inst of Tech Chennai (Indian Inst of Tech Chennai) pursuant to License Agreement. No further reproductions authorized.

FIG. 9
SEM-EDS point analysis.

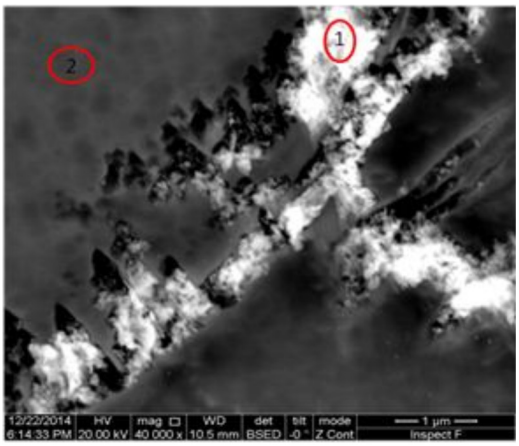

Spot	Spot 1	Spot 2
Element	Weight %	Weight %
Al	2.99	2.9
Sn	11.05	2.05
Ti	66.89	75.09
V	16.45	17.21
Cr	2.61	2.75

FIG. 10
TEM image showing the precipitates.

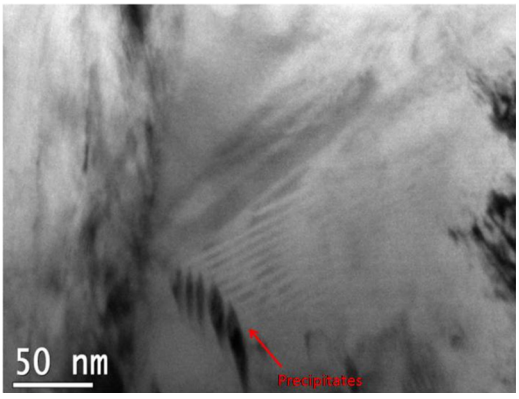

Copyright by ASTM Int'l (all rights reserved); Fri Aug 14 09:36:56 EDT 2015
Downloaded/printed by
Indian Inst of Tech Chennai (Indian Inst of Tech Chennai) pursuant to License Agreement. No further reproductions authorized.

FIG. 11 EBSD image showing the formation of precipitates.

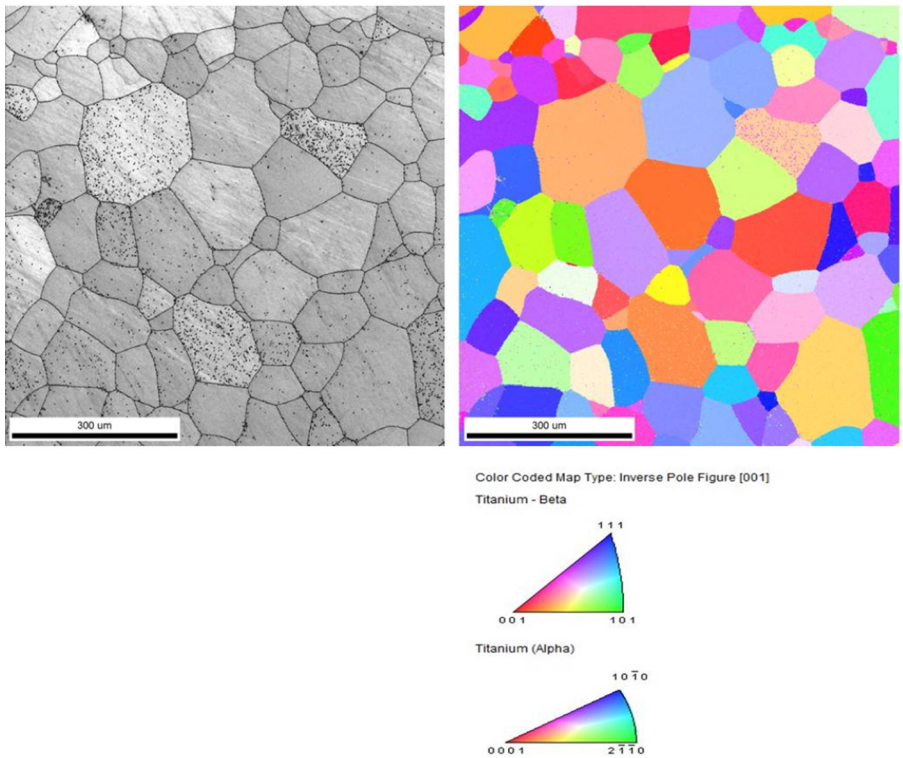

FIG. 12 EBSD image showing the formation of precipitates on triple point (8-mm continuous current condition).

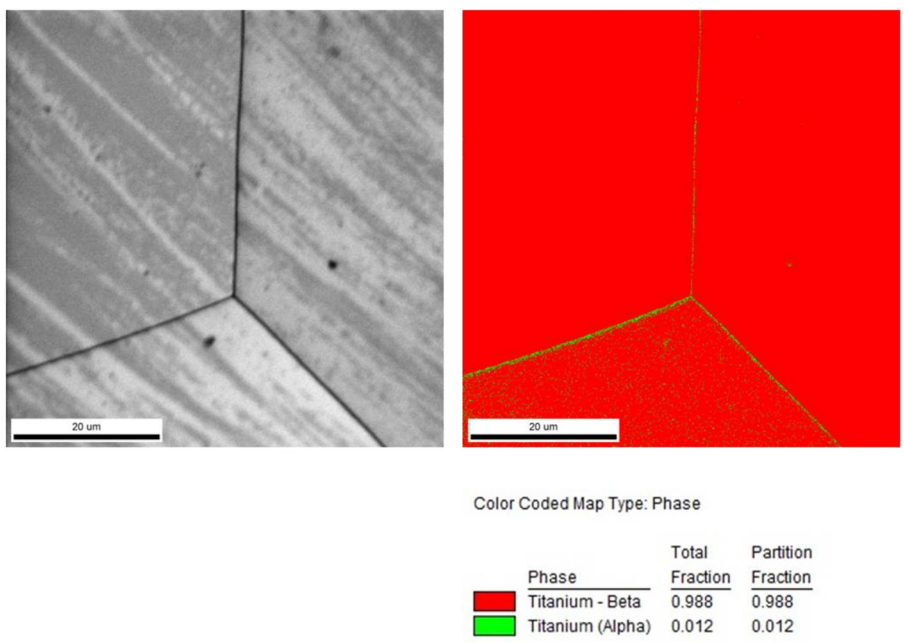

Copyright by ASTM Int'l (all rights reserved); Fri Aug 14 09:36:56 EDT 2015
Downloaded/printed by
Indian Inst of Tech Chennai (Indian Inst of Tech Chennai) pursuant to License Agreement. No further reproductions authorized.

TABLE 3

Microhardness and average grain size at various thermal cycles.

Thermal Cycle	Microhardness ($HV_{0.5}$)	Average Grain Size (mm)
Continuous current TIG, 8 mm	292.32 ± 56	139
Continuous current TIG, 10 mm	237.73 ± 23.7	110
4 Hz pulsed current TIG, 8 mm	268.17 ± 41.4	159
4 Hz pulsed current TIG, 10 mm	243.86 ± 16.12	108
6 Hz pulsed current TIG, 8 mm	248.19 ± 25.16	140
6 Hz pulsed current TIG, 10 mm	246.1 ± 18.7	80
Low cooling rate cycle (4 Hz), 8 mm	258.81 ± 15.1	176
Solution-treated condition	259 ± 18.7	96

Workflow in the Accelerated Design of New Alloys

Workflows [17] are important tools to visualize the larger picture in the integrated design of new materials. **Figure 14** shows a typical legacy workflow in the choice of the welding process and its parameters and a suggested modification. The forward direction illustrates the parametric experimental studies that start off with a choice of the welding technique and process parameters. Thermocouples or infrared pyrometers are used to estimate actual thermal profiles that prevail in the vicinity of the weld. Experimental logistics often limit how close to the weld line and at how many different locations one could capture the thermal profiles. These are then used as input parameters for HAZ simulations in Gleeble to obtain larger samples that could be characterized in detail for microstructure and mechanical properties. The reverse direction illustrates the choice of the welding technique and process parameters from the performance characteristics that come from the design of the product. The large number of experiments that form part of the forward problem renders

FIG. 13

Schematic representation of weld cooling cycle and continuous cooling transformation (CCT) curve plotted in JMAT pro with composition 75.95 wt. % Ti + 2.91 wt. % Al + 3.06 wt. % Cr + 14.79 wt. % V + 3.03 wt. % Sn.

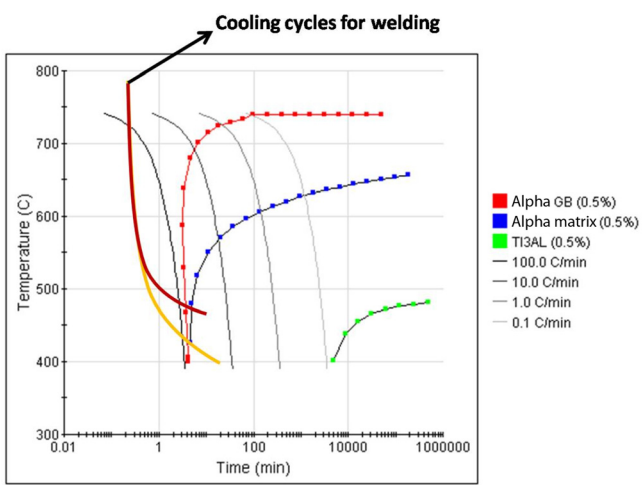

Copyright by ASTM Int'l (all rights reserved); Fri Aug 14 09:36:56 EDT 2015
Downloaded/printed by
Indian Inst of Tech Chennai (Indian Inst of Tech Chennai) pursuant to License Agreement. No further reproductions authorized.

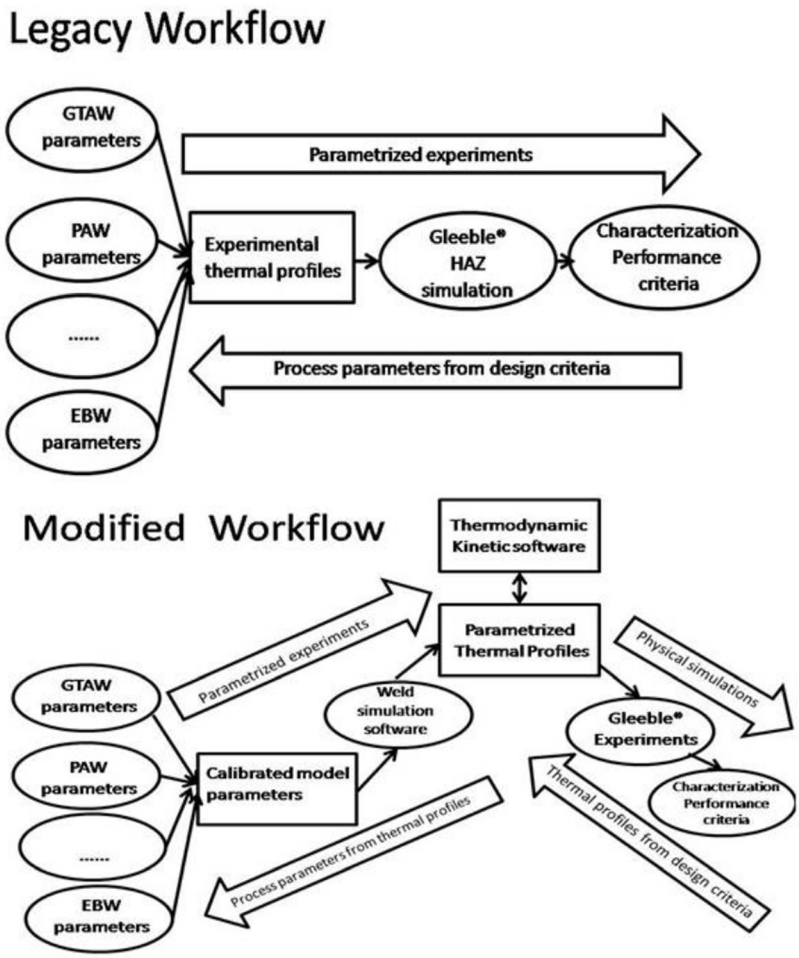

FIG. 14
Schematic workflow for integrated approach toward the design of new alloys for weldability. Legacy and suggested workflows are given.

the parametric space for the design choice large enough that soft computing tools are being resorted to [18].

In view of the strong link between the thermal profiles and the phase evolution that could be determined using CCT curves obtained from materials thermodynamics and kinetics software such as JMatPro, we suggest that the workflow could be in two segments. This is illustrated as a modified workflow in **Fig. 14**. The parametric experimental studies using different welding techniques and process parameters could be coupled with weld-simulation software to determine the model parameters that are calibrated for accurate reproduction of experimentally observed thermal profiles. Considering the maturity of the weld-simulation software commercially available, one can then assume that the thermal profiles given as output from these tools are reasonable and accurate. Once the model parameters are available, welds of any complex geometry could be taken up in the computer simulation and thermal profiles at any location could be obtained. These can then be parameterized based on the premise that such thermal profiles are not of arbitrary steps and durations as possible in post-weld heat treatment but are of (nearly) exponentially decaying in

Copyright by ASTM Int'l (all rights reserved); Fri Aug 14 09:36:56 EDT 2015
Downloaded/printed by
Indian Inst of Tech Chennai (Indian Inst of Tech Chennai) pursuant to License Agreement. No further reproductions authorized.

nature optionally superposed with thermal oscillations that arise from the nature of the heat source (arc/beam, continuous/pulsed) used. These profiles can be used along with thermodynamic and kinetic software to determine the likely microstructure in the weldment. In the absence of thermodynamic or kinetic data or for verification of microstructure evolution in known alloys, a controlled set of physical simulations could be performed using a thermomechanical simulator such as Gleeble. Though this scheme leads to the reverse problem into two stages, it is expected that the parametric space is considerably reduced to make the design choices significantly easier. It is believed that such a workflow with the strong coupling between the thermal profiles and thermo-kinetic simulations playing a pivotal role would help design new alloys for weldability in an accelerated manner.

Conclusions

An integrated study of the welding process can be performed using a combination of Sysweld software simulation and physical simulations using Gleeble. In the Ti-15-3 alloy, the grain boundary precipitates formed in all the welding cycles simulated. The amount of α precipitates formed depends on the thermal cycle, which is sensitive to the pulse frequency and the distance away from the weld centerline. Inhomogeneous precipitation of α phase across different β grains led to large scatter in the hardness profile. These aspects lead to an increase in the uncertainty of mechanical response predictions and should be taken into account in the design process. A modified workflow is suggested where the thermal profile and thermo-kinetic simulations play a pivotal role, and the process parameter space to be explored for the reverse problem of design could be reduced significantly.

ACKNOWLEDGMENTS

The writers thank the Department of Science and Technology, Government of India and Centre for Industrial Consultancy & Sponsored Research Indian Institute of Technology (ISRO-IITM) Cell for financial support through two projects that enabled acquisition of the resources used in this project. M.R.R. thanks Mr. Abhishek Kumar for assistance in experimentation.

References

[1] Schubert, E., Klassen, M., Zerner, I., Walz, C., and Sepold, G., "Light Weight Structures Produced by Laser Beam Joining for Future Applications in Automobile and Aerospace Industry," *J. Mater. Proc. Technol.*, Vol. 115, No. 1, 2001, pp. 2–8.

[2] Williams, J. C., Hickman, B. S., and Leslie, D. S., "The Effect of Ternary Additions on the Decomposition of Metastable Beta-Phase Titanium Alloys," *Metall. Trans.*, Vol. 2, No. 2, 1971, pp. 477–484.

[3] Furuhara, T., Maki, T., and Makino, T., "Microstructure Control by Thermomechanical Processing in β-Ti-15-3 Alloy," *J. Mater. Proc. Technol.*, Vol. 117, No. 3, 2001, pp. 318–323.

[4] Balachandar, K., Sarma,V. S., Pant, B., and Phanikumar, G., "Microstructure and Mechanical Properties of Gas–Tungsten–Arc-Welded Ti-15-3 Beta Titanium Alloy," *Metall. Trans. A*, Vol. 40, No. 11, 2009, pp. 2685–2693.

Copyright by ASTM Int'l (all rights reserved); Fri Aug 14 09:36:56 EDT 2015
Downloaded/printed by
Indian Inst of Tech Chennai (Indian Inst of Tech Chennai) pursuant to License Agreement. No further reproductions authorized.

[5] Eylon, D., Boyer, R. R., Koss, D. A., and Bania, P. J., "Beta Titanium Alloys in the 1990's," The Minerals, Metals & Materials Society (TMS), Warrendale, PA, 1993.

[6] Becker, D. W. and Baeslack, W. A., III, "Property-Microstructure Relationships in Metastable-Beta Titanium Alloy Weldments," *Welding Res. Suppl.*, Vol. 59, March, 1980, pp. 85s–92s.

[7] Donachie, M. J., Jr., "Ti-15V-3Cr-3Al-3Sn," *Titanium—A Technical Guide*, 2nd ed., ASM International, Materials Park, OH, 2000, p. 70.

[8] Boyer, R., Welsch, G., and Collings, E. W., "Ti-15V-3Cr-3Al-3Sn," *Materials Properties Handbook: Titanium Alloys*, ASM International, Materials Park, OH, 2007, pp. 899–920.

[9] Baeslack, W. A., III, Liu, P. S., and Paskell, T., "Weld Solidification and HAZ Liquation in a Metastable-Beta Titanium Alloy-Beta-21S," *Mater. Character.*, Vol. 30, No. 2, 1993, pp. 147–154.

[10] Pasang, T., Sánchez Amaya, J. M., Tao, Y., Amaya-Vazquez, M. R., Botana, F. J., Sabol, J. C., Misiolek, W. Z., and Kamiya, O., "Comparison of Ti-5Al-5V-5Mo-3Cr Welds Performed by Laser Beam, Electron Beam and Gas Tungsten Arc Welding," *Proc. Eng.*, Vol. 63, 2013, pp. 397–404.

[11] Bate, S. K., Charles, R., and Warren, A., "Finite Element Analysis of a Single Bead-on-Plate Specimen Using SYSWELD," *Int. J. Pres. Ves. Pip.*, Vol. 86, No. 1, 2009, pp. 73–78.

[12] Ojo, O. A. and Chaturvedi, M. C., "On the Role of Liquated γ' Precipitates in Weld Heat Affected Zone Microfissuring of a Nickel-Based Superalloy," *Mater. Sci. Eng. A*, Vol. 403, Nos. 1–2, 2005, pp. 77–86.

[13] Santhosh, R., Geetha, M., Saxena, V. K., and Nageswararao, M., "Studies on Single and Duplex Aging of Metastable Beta Titanium Alloy Ti–15V–3Cr–3-Al–3Sn," *J. Alloy Compd.*, Vol. 605, August 25, 2014, pp. 222–229.

[14] Salib, M., Teixeira, J., Germain, L., Lamielle, E., Gey, N., and Aeby-Gautier, E., "Influence of Transformation Temperature on Microtexture Formation Associated With α Precipitation at β Grain Boundaries in a β Metastable Titanium Alloy," *Acta Mater.*, Vol. 61, No. 10, 2013, pp. 3758–3768.

[15] Zhang, T., Zheng, Z., and Zhao, R., "A Dynamic Welding Heat Source Model in Pulsed Current Gas Tungsten Arc Welding," *J. Mater. Proc. Technol.*, Vol. 213, No. 12, 2013, pp. 2329–2338.

[16] Goldak, J., Chakravarti, A., and Bibby, M., "A New Finite Element Model for Welding Heat Sources," *Metall. Trans. B*, Vol. 15, No. 2, 1984, pp. 299–305.

[17] Panchal, J. H., Kalidindi, S. R., and McDowell, D. L., "Key Computational Modeling Issues in Integrated Computational Materials Engineering," *Comput. Aided Design*, Vol. 45, No. 1, 2013, pp. 4–25.

[18] Tancret, F., "Computational Thermodynamics, Gaussian Processes and Genetic Algorithms: Combined Tools to Design New Alloys," *Model. Simul. Mater. Sci. Eng.*, Vol. 21, No. 4, 2013.

Copyright by ASTM Int'l (all rights reserved); Fri Aug 14 09:36:56 EDT 2015
Downloaded/printed by
Indian Inst of Tech Chennai (Indian Inst of Tech Chennai) pursuant to License Agreement. No further reproductions authorized.